ACS PHYSICAL CHEMISTRY Au
AN OPEN ACCESS JOURNAL OF THE AMERICAN CHEMICAL SOCIETY

pubs.acs.org/physchemau
Review

Is the Future of Materials Amorphous? Challenges and Opportunities in Simulations of Amorphous Materials

Ata Madanchi, Emna Azek, Karim Zongo, Laurent K. Béland, Normand Mousseau, and Lena Simine*

Cite This: ACS Phys. Chem Au 2025, 5, 3−16
Read Online
ACCESS | Metrics & More | Article Recommendations

ABSTRACT: Amorphous solids form an enormous and underutilized class of materials. In order to drive the discovery of new useful amorphous materials further we need to achieve a closer convergence between computational and experimental methods. In this review, we highlight some of the important gaps between computational simulations and experiments, discuss popular state-of-the-art computational techniques such as the Activation Relaxation Technique *nouveau* (ARTn) and Reverse Monte Carlo (RMC), and introduce more recent advances: machine learning interatomic potentials (MLIPs) and generative machine learning for simulations of amorphous matter (e.g., MAP). Examples are drawn from amorphous silicon and silica literature as well as from molecular glasses. Our outlook stresses the need for new computational methods to extend the time- and length-scales accessible through numerical simulations.

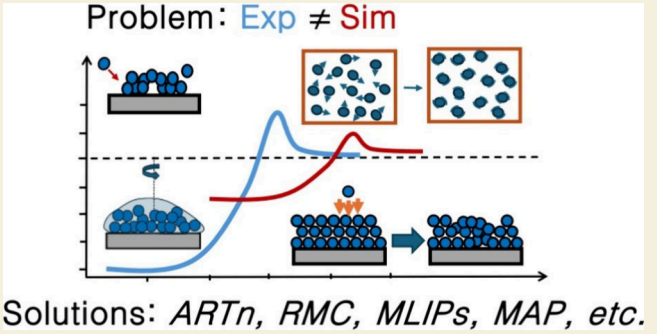

KEYWORDS: *Amorphous Materials, Computational methods, Activation Relaxation Technique nouveau, Machine Learning Interatomic Potentials, Deep Generative Models, Mesoscale Simulation, Inverse Design, Computational Material Science*

INTRODUCTION

For over a century amorphous materials remained at the forefront of pure and applied research. From theoretical and computational perspective, at the forefront are the elusive physics of the glass transition,[1] the quantification of hidden order in hyperuniform yet apparently random structures endowed with exotic properties,[2] the interpretation of characterization experiments,[3] the extension of computational simulations across multiple length- and time- scales for predictive modeling,[4−7] and the development of machine learning approaches to help design useful amorphous materials. In this review, we present some of the challenges, the state-of-the-art computational approaches, and the opportunities that drive research farther into the amorphous chemical space.

Amorphous materials are typically defined as lacking long-range order, which means their atomic structure does not produce the well-defined diffraction patterns such as those seen in crystalline solids. This lack of a sharp, periodic arrangement results in indistinctive characteristics in many characterization experiments, such as broad diffuse scattering signals. However, this does not mean that amorphous structures are entirely without order. On a short-range scale, their atomic arrangements can display local order, with atoms adopting particular bonding configurations over a few atomic distances. This local order may vary depending on whether the material is in a liquid or solid state;[8,9] the subset of amorphous structures in which the short-range order in the solid state is identical to that of the liquid phase is called glasses.

On the practical side, amorphous solids and glasses have numerous applications in biomedical engineering,[10,11] sports equipment,[12] energy conversion[13,14] and even nuclear waste immobilization through vitrification.[15] The number of potential glass compositions is estimated to be around 10^{52}, with only about 10^5 compositions realized so far.[16] The search for new compounds in this vast chemical space is enabled by sophisticated computational methods ranging from computational modeling of materials and their properties to informing search policies and hypothesis generation.

The main challenge in modeling of amorphous materials with atomistic resolution is the disconnect between lab-based and computer-based molecular structures which primarily arises due to the limited length- and time-scales accessible to atomistic simulation methods. On the technical level this is due to (1) the difficult statistical sampling in the rugged energy landscapes characteristic of amorphous matter, and (2) the

Received: August 1, 2024
Revised: December 10, 2024
Accepted: December 13, 2024
Published: December 31, 2024

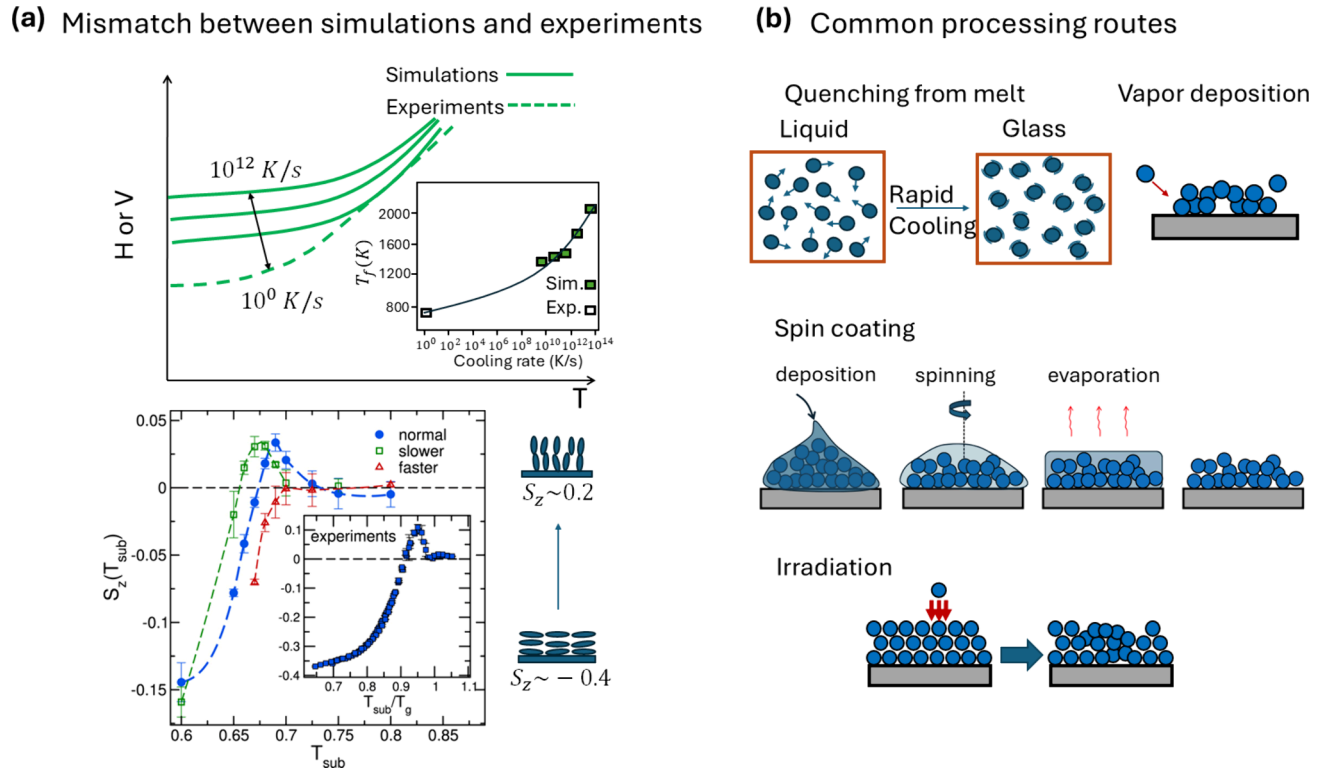

Figure 1. Summary of the existing simulation−experiment dichotomy in amorphous materials. (a) Mismatch between observable properties in simulated and real amorphous materials. (a) Top panel: Enthalpy H/Volume V as a function of temperature is schematically sketched (artist's impression) for simulations (solid lines) and for experiments (dashed lines), illustrating isobaric cooling in a generic amorphous material as a function of temperature. Simulations that mimic experimental procedures typically employ cooling rates several order of magnitude faster (10^{14}–10^{9} K/s) than those possible in traditional melt quench experiments (10^{2}–10^{0} K/s).[17−20] The inset shows fictive temperature, as a measure of stability, plotted versus cooling rate measured for silicate glasses in simulations and experiments (Reprinted from ref 18, with the permission of AIP publishing). Bottom panel: Similarly, simulated vapor deposition rates (often >10^{8} nm/s)[21−26] outpace experimental rates which are usually below 10^{0} nm/s.[27−33] The figure shows the orientational order parameter, Sz, as a function of substrate temperature, observed in both simulations[35] and experiments[37] of TPD glasses (Reprinted from ref 35, with permissions of AIP publication). While simulations qualitatively capture the nonmonotonic behavior observed in experiments there are quantitative discrepancies between simulated and experimental trends. (b) Illustrations of common processing routes for amorphous materials. Quenching from melt: A molten material is rapidly cooled (quenched) below its melting point, preventing crystallization and resulting in an amorphous solid; Vapor deposition: Atoms or molecules in a gaseous state are deposited onto a cold substrate. The rapid solidification on the surface prevents the formation of crystalline structures. Spin coating: A solution is deposited on a spinning platform where its self-assembly is governed by the interplay between surface tension, centripetal forces, and evaporation process. Irradiation: A crystalline/ceramic material is exposed to a flux of high-energy particles (e.g., ion, neutrons) resulting in an induced structural transformation.

limited physical validity of interatomic interaction models. In Part 1 of this review, we outline some of the problems that arise because of the mismatch between simulations and experiments and list the key factors that lead to the mismatch. In Part 2, we review the evolution of domain-relevant sampling methodologies over the past few decades, and finally, in Part 3, we discuss the most recent advances that propel the field forward by integrating machine learning into the simulation protocols. We conclude in Part 4 with a brief partial summary of the remaining challenges that make the field of simulation of amorphous materials particularly exciting today.

PART 1: DISCORD BETWEEN COMPUTATIONAL SIMULATIONS AND EXPERIMENTS

While massively parallel computing and, more recently, generative machine leaning models can, in principle, address the length-scale limitation of computational simulations, overcoming the time scale issue within the confines of molecular dynamics (MD) simulations— the workhorse of atomistic modeling—remains a significant challenge. Numerical methods can cover the first microsecond of reaction time, while experiments often take many orders of magnitude longer−seconds, minutes, hours. Consequently, various algorithms are employed to create computational models of amorphous materials, each exhibiting different structures and properties that often deviate significantly from those produced by experimental methods.

The isobaric enthalpy (H) versus temperature graph in the top panel of Figure 1(a) illustrates the difference in the stability of the resulting structures obtained in melt-and-quench protocols placing the simulated samples in a qualitatively higher enthalpic register. The inset illustrates this point using another measure of stability−the fictive temperature which is plotted versus cooling rate measured for silicate glasses in simulations and experiments (reproduced from ref.[34]) showing a large gap between the two.

The bottom panel in Figure 1a shows the behavior of order parameter S_z that describes the average orientation of molecules within a thin film deposited via vapor deposition as a function of substrate temperature, observed in both

https://doi.org/10.1021/acsphyschemau.4c00063
ACS Phys. Chem Au 2025, 5, 3−16

simulations[35−37] and experiments.[37,38] At high substrate temperatures ($T_{sub} > T_g$, where T_g is the glass transition temperature), the molecules exhibit random orientations, resulting in $S_z \approx 0$. As the substrate temperature decreases below T_g the molecules initially tend to align perpendicular to the substrate ($S_z > 0$). Upon further cooling, the molecular orientation transitions to a predominantly parallel alignment relative to the substrate ($S_z < 0$). While simulations qualitatively capture this nonmonotonic behavior observed in experiments, certain limitations exist. Since, deposition rate has been found to be an effective parameter in dictating the relaxation dynamics of vapor deposited glasses,[39] T_g estimated from simulations is generally higher than experimentally determined values.[40] Such discrepancies arising from simpler models and limited time/length scales influence the quantitative agreement between simulated and experimental trends.

In Figure 1b we summarize schematically some of the typical processing routes starting from those that are reasonably approachable through simulations like melt-and-quench and vapor deposition to those that are notoriously difficult to model like spin-coating and irradiation. To illustrate the depth of the fundamental simulation-experiment discrepancy, consider for example that computational models of a-Si are routinely generated using melt-and-quench MD simulations, even though a-Si cannot be fabricated in the laboratory using a melt-and-quench process.

Specific Examples of Systems of Interest

Before we dive into the discussion of computational strategies, we first provide concrete context by introducing some of the commonly studied inorganic and organic amorphous solids, their applications, and the challenges associated with their preparation and simulation.

Inorganic Amorphous Solids. Amorphous silicon (a-Si) and amorphous silica (a-SiO_2) are canonical examples of nonmetallic amorphous materials, with a-Si being a nonglassy amorphous solid and a-SiO_2 being a glassy one. Over more than 60 years of extensive research, a broad consensus has emerged regarding many of their characteristics. Both materials are considered continuous random networks with few coordination defects, existing as metastable phases possessing a free energy higher than that of their crystalline counterparts. However, their exact structure and properties are highly dependent on their processing history. From a technological perspective, this variability in structure and properties is significant for established industries, such as hydrogenated a-Si photovoltaic panels fabricated by chemical vapor deposition (CVD),[41] and critical for emerging industries, such as advanced photonics applications. Amorphous silicon, in particular, is being considered for use in photonic integrated circuits and advanced transistor devices because plasma-enhanced CVD a-Si deposition is compatible with other complementary metal−oxide−semiconductor fabrication steps, unlike traditional c-Si processing routes.[42,43] For these applications, there is a direct relationship between processing conditions and electro-optical properties, making a-Si's suitability for advanced applications highly dependent on its fabrication method.

Similarly, a-SiO_2 exhibits variations when produced by different methods, such as fusing silica crystals versus formation through irradiation. Radiation-induced changes are particularly relevant for nuclear power plant aging and nuclear waste management. Irradiation can cause significant structural changes to silicate-based aggregates in concrete, leading to dimensional changes, alterations in chemical reactivity, and modifications of mechanical properties.[44−48] The variability in processing routes also raises fundamental questions about how to define a reference "perfect" form of a-Si and a-SiO_2. Different deposition conditions and thermal treatments can significantly affect the structure of a-Si.[49−52] Even a-Si created by ion-implantation, which is often considered as a good reference because of its low porosity, can be arbitrarily relaxed by thermal treatment.[53,54] Likewise, there is clear evidence that irradiation of fused (vitreous) silica causes substantial structural changes.[55−57]

Molecular Amorphous Solids. Beyond the traditional silicate-based compositions, when cooled from a molten state small organic molecules can transition into amorphous or glassy phases that are commonly known as molecular glasses or amorphous molecular materials.[58] Molecular glasses have broad applications across various industries due to their unique properties. In pharmaceuticals, they enhance solubility and bioavailability of drugs.[59−65] In electronics, they are utilized in technologies like OLEDs,[66−72] organic photovoltaics[73−75] and nonlinear optics[76−81] offering flexibility and uniformity.

The preparation of molecular glasses primarily involves three techniques: Liquid-quenching methods, spin-coating, and physical vapor deposition (PVD). Liquid-quenching involves rapid cooling which prevents crystallization and results in a metastable glassy state.[82−84] Spin coating is a technique used to deposit uniform layers of organic materials onto substrates by rapidly spinning them, ensuring precise control over film thickness and surface morphology.[27,85−87] This process is widely employed in the fabrication of organic thin-film devices such as OLEDs,[27,85,88−92] while PVD entails the evaporation or sublimation of a material in a vacuum chamber, where it condenses onto a substrate to form a glassy thin film.[93] Interest in investigating the properties and applications of vapor-deposited molecular glasses stems from their superior qualities compared to conventional glasses formed through solution processing,[27] notably their ultrastability.[21,28−31,94] Vapor-deposited molecular glasses offer higher density,[95−97] unique phase transitions,[95,98,99] improved mechanical properties[100−102] and anisotropy.[27,31,35,37,71,87,91,103−124] Anisotropy in these glasses is evident in their optical birefringence,[27,37,106,108,113,117,118] magnetic behavior,[103] and structural characteristics.[31,87,91,104,105,109,111,113,114]

Understanding the interplay between structural anisotropy and glass stability is critical, as it is influenced by molecular structure and deposition conditions. Structural anisotropy in PVD glasses is largely attributed to preferred molecular orientation[31,109,125] and molecular layering.[105,111,115] At low deposition temperatures (T_{dep}), molecules tend to orient horizontally (parallel to the substrate).[31] At intermediate T_{dep}, elongated molecules typically orient vertically (perpendicular to the substrate).[113] Deposition near the glass transition temperature (T_g), at slow deposition rates, or with molecules possessing smaller aspect ratios, tends to result in isotropic packing.[122,123] Both experimental and simulation studies indicate that this orientational anisotropy originates from the structure of the supercooled liquid near the surface[35,37,113,123] and stable glasses are formed through surface-mediated equilibrium during PVD,[28,126−131] where molecules near the surface have enhanced mobility allowing them to sample a

https://doi.org/10.1021/acsphyschemau.4c00063
ACS Phys. Chem Au 2025, 5, 3−16

large number of configurations in search of a more stable state. Thereby, the properties of these glasses can be controlled by adjusting deposition parameters.[38,71,122,132]

Computational Challenges

Understanding the relationship between processing conditions and structural properties is essential for optimizing the performance of glassy organic and inorganic films in various technological applications. While computational models based on Molecular Dynamics (MD) and Monte Carlo (MC) simulations offer valuable insights into the properties and behavior of molecular glasses,[4,21−23,133] there remains a vast gap between these models and real-world laboratory conditions for glass preparation, see Table 1 for the summary of discrepancies in system size and accessible time scales in simulation and experiments.

Table 1. Comparative Analysis of Key Aspects between Simulations and Experiments in the Study of Molecular Glasses

Aspect	Simulations	Experiments
System size	10^2−10^6 molecules	∼10^{23} molecules
Time scale	10^{-12}−10^{-6} s	>10−10^5 s
Deposition rate	10^8−10^{11} nm/s	10^{-2}−10^{-1} nm/s
Cooling rate	10^9−10^{14} K/s	10^0−10^2 K/s
Film thickness	<10 nm	10^2−10^4 nm

Most notably, glasses simulations remain plagued by a series of challenges:

(i) System size. Due to high computational costs, a significant disparity exists between the system sizes accessible through simulations and those investigated experimentally. Glass simulations are typically limited to relatively small scales, involving systems that range from a few hundred to several thousand molecules/particles.[133,134] In contrast, experimental studies can probe much larger systems, often extending to macroscopic dimensions encompassing 10^{23} molecules/particles or more. This difference highlights a key challenge: simulations, while providing detailed atomic-level insights, are constrained in capturing the full complexity and variability of real glassy materials, which can limit their applicability and accuracy in replicating experimental conditions.[134] Other challenges include insufficient statistical sampling with too few molecules,[135,136] enhanced thermodynamic fluctuations (which scale inversely with the square root of particle count),[137,138] and errors from limited simulation box sizes that fail to capture large structural features.[139,140] To balance accuracy and computational feasibility, the system size must be optimized to minimize finite-size effects while maintaining reasonable computational demands.

(ii) Limited accessible time scales. MD simulations are constrained to short time scales, typically up to a few microseconds,[17] whereas experimental processes can span for hours or days.[28,31,100] This disparity results in MD simulations employing ultrafast cooling rates (10^{14}−10^9 K/s), far exceeding those in conventional experiments (10^2−10° K/s).[17−20] Consequently, glasses prepared via MD tend to have higher fictive temperatures, making them less stable than experimentally synthesized glasses.[20]

For glasses prepared via melt and quench route, the rapid cooling leads to glasses that are less stable and more disordered, remaining in high-energy states. This significant difference in cooling rates between simulations and experiments creates a systematic gap, leading to less stable simulated glasses compared to their experimental counterparts.

On the other hand, for PVD glasses, deposition rates in simulations are also significantly higher (often higher than 10^8 nm/s)[21−26] compared to experimental rates (typically less than 10^0 nm/s).[27−33] This discrepancy means that simulated films tend to have different microstructures and properties compared to experimentally deposited films.[23,35] These differences in deposition rates further exacerbate the divergence in film thickness (typically, in simulations, film thicknesses are generally less than 10 nm,[21,24,25] whereas in experiments, they range from hundreds of nanometers[29,32,33] to micrometers,[31,39,76,79,100,101] see Table 1) and structural properties between simulations and experiments, as the rapid deposition does not allow for the same relaxation and ordering processes that occur in experimental conditions.[39]

Going beyond mimicking experimental protocols, and adding to the challenge, amorphous structures, with their intricate details influenced by preparation methods, have long posed fundamental questions regarding their most relaxed configuration and associated inherent features. These may or may not correspond to the structural properties of the optimal continuous random network, which is defined as the lowest strain perfectly coordinated large-scale network that can exist. While such structure is, by definition, elusive, it has oriented modeling efforts even when looking at specific materials. For example, early attempts to manually create amorphous silicon transitioned to sophisticated computational approaches, such as the bond-switching method by Wooten, Winer, and Weaire (WWW) for producing as close to perfectly coordinated optimal continuous random network compatible with silicon local bonding environment. Other significant techniques discussed in detail in Part 2 of this review, such as the Activation-Relaxation Technique nouveau (ARTn), Reverse Monte Carlo (RMC), swap Monte Carlo (SMC) have partially advanced our understanding of the relaxation mechanisms and energy landscapes of these materials measuring success both by matching experimental results and closeness to the best available CRNs.

(iii) Lack of accurate interatomic interaction potentials. Finally, the accuracy of interatomic interaction models remains limited. The electronic Density Functional Theory (DFT), a class of ab initio methods, is commonly regarded as the gold standard for modeling the potential energy surfaces (PESs) of amorphous materials. However, even at the DFT level, the use of different exchange-correlation functionals can result in significantly different PESs, leading to models with varying structures and properties. Moreover, exploring the DFT PES is computationally expensive, severely limiting the accessible length and time scales. As a result, classical interatomic interaction potentials are often employed, introducing further discrepancies between computational models and real-world amorphous materials.

Empirical force fields involve optimizing hundreds or thousands of parameters.[141,142] Even simpler classical force fields require dozens of parameters, increasing with the number of elements involved.[143] This high dimensionality complicates the identification of what would be the optimal structures based on the values in the cost function landscape of a continuous random network or the best match to experimental results.[155] In addition, the cost function landscape for force field optimization is typically rough and filled with numerous

https://doi.org/10.1021/acsphyschemau.4c00063
ACS Phys. Chem Au 2025, 5, 3−16

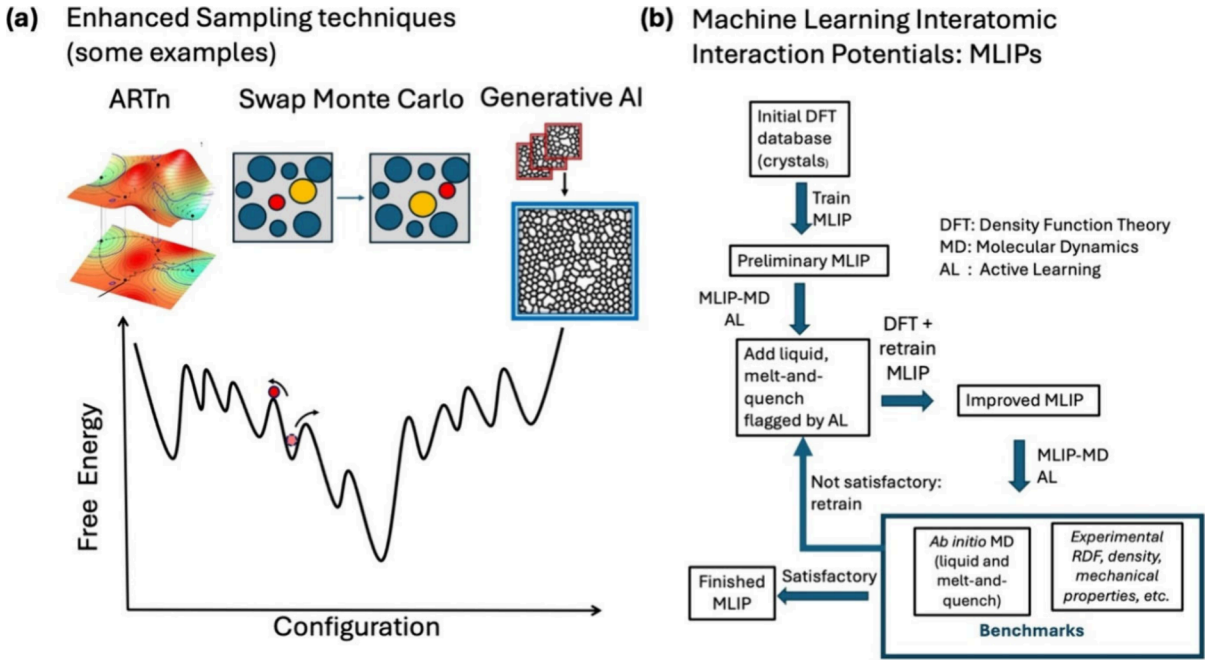

Figure 2. Illustration of computational methodologies used in sampling and potential energy modeling. (a) Featured free energy landscape of amorphous materials requires specialized enhanced sampling techniques such as ARTn, Monte Carlo, and, more recently, approaches based on generative artificial intelligence (AI). (b) Flow-chart of development of machine learning interatomic potentials (MLIPs) using ab initio methods, molecular dynamics (MD) simulations, and active learning (AL).

local minima.[144] As a result, traditional optimization methods, such as gradient descent, often get trapped in these local minima, making the process highly dependent on the initial starting point.[145] This roughness necessitates numerous independent optimizations and relies heavily on intuition, making the parametrization process biased and laborious.[143,146]

In the past decade, machine-learning (ML) potentials trained on DFT data have helped narrow this gap, see Part 3 in this review for more details. However, challenges remain, particularly concerning interfaces, chemical changes, and charge transfer.

PART 2: BEYOND MIMICKING EXPERIMENTAL PROTOCOLS: SAMPLING AND THE SEARCH FOR OPTIMAL STRUCTURE

As mentioned before, while the structural details of amorphous configurations depend on the preparation procedures, fundamental questions arose very early on as to the nature and existence of the optimal continuous-random network (CRN) structure, its features, and its generality in representing real systems. Representing thermodynamic ensembles, such structures could be produced through nondynamical processes driven only by energy or structural deformation (bond length, bond angle and coordination, for example).

If for materials such as silica, a glass characterized by significant topological rigidity near the rigidity transition threshold,[146] even short molecular dynamical procedures can lead to low-stress and low-defect structures.[147] Finding low-energy structures in high-connectivity structures is a more significant challenge that amounts to overcoming barriers in a featured free energy landscape, see Figure 2a for an illustration. For a pedagogical review on rigidity and mechanical stability of amorphous solids see ref.[148]

While the reader is referred to the recent review by Laurent J. Lewis[149] for an extensive historical account of modeling amorphous silicon, we focus here on providing a high-level view of the various approaches used to generate high-quality disordered structures beyond the generic quench and melt. In the case of glasses, we similarly refer the reader to the review of Michoulaut and Bauchy, which describes how rigidity theory can be employed to study and generate glassy silicate models.[150]

Initial attempts to create such structures for amorphous silicon were done "by hand" by Polk[151] and a few others in early 1970s. This was followed soon after by computer approaches. Among the early success is the ingenious bond-switching approach proposed by Wooten, Winer and Weaire (WWW)[152] to create a disordered network starting from a perfect crystal while preventing the creation of coordination defects using a harmonic Keating potential.[153]

The WWW algorithm was used, in its original form,[154] and revised versions that greatly accelerated the sampling allowing the generation of high-quality model of 4000[155] to 100,000 atom models that have remained reference models until today.[156] These methods were also used, iterating with relaxations using a modified Stillinger-Weber potential[157] adapted to reproduce amorphous silicon structures,[158] to generate near hyperuniform continuous-random network models.[159] While the original WWW algorithm does not impose evenness on the loops connecting atoms, it is possible to modify the method to force even cycles and explore the effects of additional chemical ordering on the structure of binary amorphous semiconductors such as a-GaAs,[160] showing the richness of this bond-switching approach to explore fundamental questions about the nature of CRNs. And while the general WWW approach produces the lowest energy structures without coordination defects, the bond-switching moves require crossing high energy barriers that are unphysical. Moreover, experimental evidence even for well-relaxed a-Si shows a significant concentration of low-

https://doi.org/10.1021/acsphyschemau.4c00063
ACS Phys. Chem Au 2025, 5, 3−16

coordination defects[161] that need to be reproduced by modeling.

In general, defects in amorphous materials include the deviations from a perfect bonding configuration,[162] dangling or floating bonds,[163] and vacancies,[164] local strain-related defects[165] may modify physical and chemical properties of the material.[166,167] In the past computational studies of defects explored the topological satisfaction of local structures using the atomic-level stresses[164,168] identified locally favored structures,[169] and examined local vibrational modes.[170,171]

Two general approaches were applied to a-Si to address this issue: Reverse Monte Carlo and the Activation-Relaxation Technique. Reverse Monte Carlo (RMC), first applied to a-Si in 1993,[172] aimed at extracting local atomic structure from global experimental averages such as the radial distribution function, using the minimum number of additional constraints. Unlike MD simulations, which depend on interatomic potentials and attempt to replicate real-time dynamics, RMC aims to find atomic configurations that match experimental data without accounting for atomic interactions or thermodynamics.[142] In RMC, atomic positions are randomly adjusted to minimize a cost function representing the difference between the model's pair correlation function and the experimental data. This process follows an accept-reject protocol, similar to the Metropolis Monte Carlo algorithm, but with a key distinction: while Metropolis Monte Carlo uses potential energy as the cost function, RMC uses the discrepancy between the simulated and experimental signals[173,174] thereby RMC avoids the high cooling rates and approximations associated with MD's force fields by bypassing the need for melt-quenching. However, its reliance on experimental data limits its predictive power, as it can only replicate structures for conditions that have already been explored.[130]

A significant challenge in RMC is that it generates atomic configurations by inverting experimental data, which often results in nonunique solutions. Different atomic arrangements can produce similar or indistinguishable experimental fingerprints, such as g(r).[143,144] This ambiguity is especially problematic for complex materials like glasses, where multiple valid yet potentially thermodynamically unstable structures may satisfy the same experimental constraints.[130,143,145] Through multiple trials, it was discovered that the range of configurations able to reproduce macroscopically averaged experimental data included a large fraction of nonphysical configurations and that the inclusion of strict constraints of local configurations was necessary to generate models close to those obtained by quench and melt.[175]

Further improving on these methods, Drabold and collaborators introduced the "Force-Enhanced Atomic Refinement" (FEAR) method to improve RMC results by recursively optimizing the structure against local classical force field-based[176] or quantum-mechanical DFT-based[177] potentials and global experimental results.[178] While the final configuration meets both constraints, often classical mechanics fails to provide adequate accuracy, and resorting to quantum-mechanical approaches limits the system sizes to only a few hundred atoms.[179] This limits greatly the advantage of this method for generating relevant samples given the local configurational richness of disordered systems such as a-Si. RMC and related techniques are further discussed in Part 3 in the context of using experimental data to inform simulations.

The Activation-Relaxation Technique nouveau (ARTn), an open-ended method for finding local transition states surrounding a local minimum,[180,181] was used to explore the energy landscape, identifying the relaxation mechanisms, and relax the structure of amorphous materials, including a-Si,[182,183] a-GaAs[184] and silica glass.[185] As with molecular dynamics, the resulting low-energy structures correspond to low-energy points of the potential energy used. The validity of the result is therefore determined by the quality of the potential. ARTn, just as the WWW algorithm, does not describe real kinetics, but rather generates activated mechanisms that can be accepted or rejected using, for example, a Metropolis criterion. However, it allows for the generation of a much broader set of mechanisms[186] that provide a better understanding the relaxation mechanisms and provides different pathways to low energy structures, an essential feature to assess the universal properties of optimal CRNs.

In the context of glass transition studies[4] that aim to explore relaxation processes in increasingly viscous substances, Swap Monte Carlo (SMC) pioneered by Grigera and Parisi[187] has become popular as it speeds up relaxation by introducing nonphysical moves that involve swapping physically distant particles. Enhanced efficiency is usually attributed to overcoming kinetic barriers typical in glass formers,[188] but it also comes with some disadvantages: it has been shown that SMC leads to artificial crystallization in some systems.[189,190] For instance, Brumer and Reichman found that while SMC was efficient for a two-dimensional hard disk system, 3D polydisperse systems were prone to phase separation/crystallization.[189] Formation of such ordered phases is an unwanted artifact because the resulting structures no longer represent the glassy state of interest. A breakthrough was achieved when Ninarello et al. demonstrated that by carefully tuning the interaction potentials and polydispersity, a set of glass formers can be studied, with speed up thermalization up to 10 orders of magnitude without crystallization.[191] SMC has since been successfully applied in numerous studies such as measuring the static length scales,[192,193] and generating ultrastable glasses.[194,195]

Although, as discussed in ref.,[191] SMC's effectiveness is quite restricted, in recent years, adaptive methods augmented by machine learning protocols, such as reinforcement learning and normalizing flows have shown that proposal distributions in Metropolis-Hasting algorithm can enhance the sampling efficiency particularly in systems where the equilibration suffers from slow dynamics and metastability.[196,197] Thanks to the ongoing intensive method development in the MC community, for example ref.[198] we expect to see more novel designs of MC methods accompanied by "smart" moves in context of amorphous materials and glasses in near future.

PART 3: NEW IDEAS: MACHINE LEARNING FOR IMPROVED ACCURACY, SAMPLING, AND REDUCED MISMATCH WITH EXPERIMENTS

Machine Learning Interatomic Potentials

Atomistic simulations, powered by machine learning interatomic interaction models, revolutionize materials science in unprecedented ways[199,200] lifting many barriers in modeling. None of these barriers, from the spatiotemporal limitation of density function theory to the transferability limitations of semiempirical models pose a problem for machine learning interatomic potentials (MLIP). While several MLIP models have been developed since the first one by Bheler et al. in 2007[201] they all rely on approximations of the potential energy

https://doi.org/10.1021/acsphyschemau.4c00063
ACS Phys. Chem Au 2025, 5, 3−16

surface (PES). This approximation assumes a medium without charge or polarization, allowing the total energy of a given system to be approximated by the sum of individual atomic energies. These individual energies strongly depend on the local atomic environment, which is captured by descriptors representing the surrounding atomic configurations.[202]

This concept, in principle, is based on atomic environment descriptors, regression methods, and quantum mechanical data.[203,204] Except for the symmetry of the Hamiltonian, there is no direct parametrization based on the type of physical interactions. Instead, it relies on mathematical interpolation of the potential energy surface (PES), utilizing quantum mechanical data that constitutes a set of discrete points on the PES. Thus, the accuracy of MLIP depends on how well these discrete points cover the targeted PES, a problem that is often addressed by resorting to active learning protocols.

The flow-chart in Figure 2b outlines a typical MLIP training protocol. MLIPs differ based on the type of local atomic environment descriptors and regressors used. Current regression methods can be grouped into three main categories: artificial neural networks (NNs),[201,205] kernel-based method,[206] and linear regression.[207,208] The first two categories have been employed in modeling amorphous silicon (a-Si) and amorphous silica (a-SiO2) using neural network potentials and Gaussian approximation potentials.[209−213] Linear regression potentials include the Spectral Neighbor Analysis Potential (SNAP),[207] atomic cluster expansion[214] and the Moment Tensor Potential (MTP).[208] These have recently been leveraged in order to create MLIPs able to jointly describe Si, SiO_2 and their interfaces,[213,215,216] in solid, liquid and amorphous states, with a very good level of fidelity.

Sampling

Approaches based on machine learning are enriching the search for both experimentally relevant and optimal structures. As mentioned above, progress for the former, was made with the development of DFT-quality machine-learned potentials that made it possible to generate well-relaxed large amorphous models with low defects using quench and melt approaches.[206,217] Coupled with recent large-scale melt-and-quench work using the modified Stilliger-Weber potential,[218] this work demonstrates that with the right potential and sufficient computational effort, it is possible to generate structure that, while presenting some coordination defects, are comparable in structure to the best continuous random networks (CRNs) generated using the Wooten, Winer and Weaire (WWW) approach.

Nevertheless, fundamental questions remain: the minimum strain structure that can be generated - how does it vary with size? After all the work needed to relax a structure to the same level as WWW increases faster than the number of atoms, as seen in ref.,[155] for example; what of binary network, etc.? To answer these questions, Comin and Lewis developed a machine-learning approach to directly generate a-Si structures after learning from high-quality models.[219] If the initial results are still far from optimal, they show that this task is possible with sufficient training data and the right ML model. Indeed, in recent years a variety of generative models have been explored, including GANs refs,[220,221] autoencoders,[219] normalizing flows.[222] Following the work of Comin and Lewis, GAN models have been used to generate amorphous structures based on point cloud representations of molecular input.[221]

The fast-decaying structural correlations characteristic of amorphous materials suggest that autoregressive generation may be an effective strategy for sampling large scale amorphous configurations. In an autoregressive approach, the probability of transitions from one microstate to others is inferred from small-scale (order of correlation length) samples of the material. Then the larger sample is extrapolated from small samples, and it is generated one grid-point at a time conditional on previously generated molecular context. The cost of sampling is thereby limited to linear scaling with the number of populated grid points. Recent works in this area developed a modeling approach called the Morphological Autoregressive Protocol (MAP) based on the PixelCNN architecture[223,224] with grid-based representation of molecular structures showing promising results on systems like amorphous graphene (2D), and liquid water (3D). Grid-based input representation offers the benefits of easy processing and, in the case of 2-dimensional films, the possibility of direct integration of experimental microscopy data into the modeling loop; but comes with high memory demands. As an alternative, point cloud representations offer scalability but require careful design to ensure symmetry invariance.[225,226]

Informing Simulations Using Experimental Data

The gap between simulation and experiment may be reduced by integrating experimentally measured parameters into simulations. This may be done by including experimental data as simulation parameters[176,178,227] or as constraints.[228−230] For instance, molecular dynamics simulations of amorphous silicon (a-Si) and amorphous silica (a-SiO_2) are initialized using experimental structural data such as atomic coordinates and lattice parameters.[228−231] These are usually determined experimentally via techniques such as X-ray crystallography[232,233] and neutron diffraction.[234,235] Furthermore, a cubic box corresponding to the experimental density of amorphous silica (2.20 g/cm^3) was used to prepare the amorphous silica components of the MLIP databases.[142,236,237]

Experimental data obtained from diffraction, infrared (IR), and nuclear magnetic resonance (NMR) measurements is used constraints to minimize a cost function during the simulation of a-Si and a-SiO2 within the framework of Reverse Monte Carlo (RMC)[238,239] and related Hybrid Reverse Monte Carlo (HRMC).[240,241] For example, experimental structure factors, Si−Si−Si bond angles, and density data were used as constraints to simulate amorphous silicon with the standard Reverse Monte Carlo (RMC) method.[242] In addition, realistic amorphous silica structures may be generated using the RMC method by applying experimental constraints such as Si−O bonds, intratetrahedral (O−Si−O) bond angles, and intertetrahedral (Si−O−Si) bond angles.[243] The HRMC method encompasses, but is not limited to, Experimentally Constrained Molecular Relaxation (ECMR),[244] Experimentally Constrained Structural Relaxation (ECSR),[245] and Force-Enhanced Atomic Refinement (FEAR).[176] Both a-Si and a-SiO_2 were successfully simulated with high fidelity within these frameworks. For instance, in ECSR, the experimental reduced electron diffraction intensities and the experimental fluctuation electron microscopy FEM variance data were used.[245] The FEAR method was successfully applied to both a-Si and a-SiO2 using the pair distribution function obtained from neutron diffraction and X-ray diffraction data as experimental constraint.[176] These approaches may be applied to molecular

https://doi.org/10.1021/acsphyschemau.4c00063
ACS Phys. Chem Au 2025, 5, 3−16

glasses, but molecular glasses remain at earlier stages of computational exploration than amorphous silica and silicon.[58]

PART 4: CONCLUSIONS AND OUTLOOK

In this review, we examined the pivotal role of computational simulations in bridging the gap between theoretical predictions and experimental observations. We highlighted significant advancements in modeling amorphous materials, including a-Si, a-SiO_2, and molecular glasses, while acknowledging the ongoing challenges related to matching the experimentally relevant system sizes and time scales.

Until recently computational simulations of amorphous materials reflected a choice of either accepting artifacts that arise due to inadequately small size of the simulated systems studied on time scales that are too short using methods that are too expensive to scale up or accepting the artifacts of the inaccuracies that come with reliance on force-fields/purely data-driven techniques. In this review we explored the progress in conformation sampling methods, from techniques that mimic experimental protocols such as the traditional quenching and melting and vapor deposition techniques to more general approaches such as Reverse Monte Carlo (RMC) and the Activation-Relaxation Technique nouveau (ARTn), to the novel machine learning-based approaches developed specifically for amorphous materials, including generative models and autoregressive techniques such as the Morphological Autoregressive Protocol (MAP). Finally, we have discussed a recent development that is of particular importance to the field of amorphous matters—the emergence of machine learning interatomic potentials (MLIPs) that bring DFT-level accuracy to atomistic simulations at a reduced cost relative to DFT, augmenting simultaneously the accuracy and sampling efficiency.

The advances discussed in this review bring us closer to the ultimate goal of informing experiments using computational simulations and guiding and accelerating the design of useful amorphous materials. New ideas, however, are still needed to completely close the gap in time- and length- scales between simulations and experiments. The exciting promise of this field is that by constructing new methods we may unlock an incomprehensively enormous set of new chemical species. And while it may not yet be widely appreciated, to us the future of materials appears to be delightfully amorphous.

AUTHOR INFORMATION

Corresponding Author

Lena Simine − *Department of Chemistry, McGill University, Montréal, Québec H3A 0B8, Canada;* orcid.org/0000-0002-8188-0550; Email: lena.simine@mcgill.ca

Authors

Ata Madanchi − *Department of Physics, McGill University, Montréal, Québec H3A 2T8, Canada*

Emna Azek − *Department of Chemistry, McGill University, Montréal, Québec H3A 0B8, Canada*

Karim Zongo − *Department of Mechanical and Materials Engineering, Queen's University, Kingston, ON K7L 3N6, Canada*

Laurent K. Béland − *Department of Mechanical and Materials Engineering, Queen's University, Kingston, ON K7L 3N6, Canada;* orcid.org/0000-0001-5332-7128

Normand Mousseau − *Département de Physique, Institut Courtois and Regroupement Québécois sur les Matériaux de Pointe, Université de Montréal, Montréal, Québec H3C 3J7, Canada*

Complete contact information is available at: https://pubs.acs.org/10.1021/acsphyschemau.4c00063

Author Contributions

The manuscript was written through contributions of all authors and all authors have given approval to the final version of the manuscript.

Funding

National Research Council via the AI4Design program, NSERC Alliance Grants - Consortia Quantum "QuantaMole" and NSERC Discovery Grant, IVADO, Nuclear Waste Management Organization of Canada.

Notes

The authors declare no competing financial interest.

ACKNOWLEDGMENTS

A.M., E.A., and L.S. acknowledge funding from the National Research Council via the AI4Design program, NSERC Alliance Grants - Consortia Quantum "QuantaMole", and IVADO. L.B. and K.Z. acknowledge support from NSERC and the Nuclear Waste Management Organization of Canada. N.M. acknowledges partial support from a NSERC Discovery Grant.

REFERENCES

(1) Berthier, L.; Biroli, G. Theoretical perspective on the glass transition and amorphous materials. *Rev. Mod. Phys.* **2011**, *83* (2), 587−645.

(2) Torquato, S. Hyperuniformity and its generalizations. *Phys. Rev. E* **2016**, *94* (2−1), 022122.

(3) Montoya-Castillo, A.; Chen, M. S.; Raj, S. L.; Jung, K. A.; Kjaer, K. S.; Morawietz, T.; Gaffney, K. J.; van Driel, T. B.; Markland, T. E. Optically Induced Anisotropy in Time-Resolved Scattering: Imaging Molecular-Scale Structure and Dynamics in Disordered Media with Experiment and Theory. *Phys. Rev. Lett.* **2022**, *129* (5), 056001.

(4) Berthier, L.; Reichman, D. R. Modern computational studies of the glass transition. *Nat. Rev. Phys.* **2023**, *5* (2), 102−116.

(5) Schleder, G. R.; Padilha, A. C. M.; Acosta, C. M.; Costa, M.; Fazzio, A. From DFT to machine learning: recent approaches to materials science−a review. *J. Phys.: Materials* **2019**, *2* (3), 032001.

(6) Salahub, D. R. Multiscale molecular modelling: from electronic structure to dynamics of nanosystems and beyond. *Phys. Chem. Chem. Phys.* **2022**, *24* (16), 9051−9081.

(7) Izvekov, S.; Voth, G. A. A multiscale coarse-graining method for biomolecular systems. *J. Phys. Chem. B* **2005**, *109* (7), 2469−73.

(8) Gupta, P. K. Non-crystalline solids: glasses and amorphous solids. *J. Non-Cryst. Solids* **1996**, *195* (1−2), 158−164.

(9) Filipponi, A.; Di Cicco, A. Short-range order in crystalline, amorphous, liquid, and supercooled germanium probed by x-ray-absorption spectroscopy. *Phys. Rev. B* **1995**, *51* (18), 12322−12336.

(10) Hua, N.; Huang, L.; Chen, W.; He, W.; Zhang, T. Biocompatible Ni-free Zr-based bulk metallic glasses with high-Zr-content: compositional optimization for potential biomedical applications. *Mater. Sci. Eng. C. Mater. Biol. Appl.* **2014**, *44*, 400−10.

(11) Kinser, E. R.; et al. Nanopatterned Bulk Metallic Glass Biosensors. *ACS Sens* **2017**, *2* (12), 1779−1787.

(12) Khun, N. W.; Yu, H.; Chong, Z. Z.; Tian, P.; Tian, Y.; Tor, S. B.; Liu, E. Mechanical and tribological properties of Zr-based bulk metallic glass for sports applications. *Mater. Des.* **2016**, *92*, 667−673.

(13) Tarigan, H. J.; Kahler, N.; Ramos, N. S.; Kumar, G.; Bernussi, A. A. Low reflectance of nano-patterned Pt-Cu-Ni-P bulk metallic glass. *Appl. Phys. Lett.* **2015**, *107* (2), 021903.
(14) Uzun, C.; Meduri, C.; Kahler, N.; de Peralta, L. G.; McCollum, J.M.; Pantoya, M.; Kumar, G.; Bernussi, A.A. Photoinduced heat conversion enhancement of metallic glass nanowire arrays. *J. Appl. Phys.* **2019**, *125* (1), 094306.
(15) McCloy, J. S.; Goel, A. Glass-ceramics for nuclear-waste immobilization. *MRS Bull.* **2017**, *42* (03), 233−240.
(16) Zanotto, E. D.; Coutinho, F. A. B. How many non-crystalline solids can be made from all the elements of the periodic table? *J. Non-Cryst. Solids* **2004**, *347* (1−3), 285−288.
(17) Lane, J. M. Cooling rate and stress relaxation in silica melts and glasses via microsecond molecular dynamics. *Phys. Rev. E Stat. Nonlin. Soft. Matter. Phys.* **2015**, *92* (1), 012320.
(18) Li, X.; et al. Cooling rate effects in sodium silicate glasses: Bridging the gap between molecular dynamics simulations and experiments. *J. Chem. Phys.* **2017**, *147* (7), 074501.
(19) Vollmayr, K.; Kob, W.; Binder, K. Cooling-rate effects in amorphous silica: A computer-simulation study. *Phys. Rev. B Condens. Matter.* **1996**, *54* (22), 15808−15827.
(20) Vollmayr, K.; Kob, W.; Binder, K. How do the properties of a glass depend on the cooling rate? A computer simulation study of a Lennard-Jones system. *J. Chem. Phys.* **1996**, *105* (11), 4714−4728.
(21) Leoni, F.; Martelli, F.; Royall, C.P.; Russo, J. Structural Signatures of Ultrastability in a Deposited Glassformer. *Phys. Rev. Lett.* **2023**, *130* (19), 198201.
(22) Yoo, D.; Song, H.; Youn, Y.; Jeon, S. H.; Cho, Y.; Han, S. A molecular dynamics study on the interface morphology of vapor-deposited amorphous organic thin films. *Phys. Chem. Chem. Phys.* **2019**, *21* (3), 1484−1490.
(23) Degitz, C.; Konrad, M.; Kaiser, S.; Wenzel, W. Simulating the growth of amorphous organic thin films. *Org. Electron.* **2022**, *102*, 106439.
(24) Reid, D. R.; Lyubimov, I.; Ediger, M. D.; de Pablo, J. J. Age and structure of a model vapour-deposited glass. *Nat. Commun.* **2016**, *7*, 13062.
(25) Muccioli, L.; D'Avino, G.; Zannoni, C. Simulation of vapor-phase deposition and growth of a pentacene thin film on C60 (001). *Adv. Mater.* **2011**, *23* (39), 4532−4536.
(26) Grigoriev, F. V.; Sulimov, V.B. Atomistic Simulation of Physical Vapor Deposition of Optical Thin Films. *Nanomaterials* **2023**, *13* (11), 1717.
(27) Shibata, M.; Sakai, Y.; Yokoyama, D. Advantages and disadvantages of vacuum-deposited and spin-coated amorphous organic semiconductor films for organic light-emitting diodes. *J. Mater. Chem. C* **2015**, *3* (42), 11178−11191.
(28) Swallen, S. F.; Kearns, K. L.; Mapes, M. K.; Kim, Y. S.; McMahon, R. J.; Ediger, M. D.; Wu, T.; Yu, L.; Satija, S. Organic Glasses with Exceptional Thermodynamic and Kinetic Stability. *Science* **2007**, *315* (5810), 353−356.
(29) Qiu, Y.; Dalal, S. S.; Ediger, M. D. Vapor-deposited organic glasses exhibit enhanced stability against photodegradation. *Soft Matter.* **2018**, *14* (15), 2827−2834.
(30) Rodriguez-Tinoco, C.; Gonzalez-Silveira, M.; Ramos, M. A.; Rodriguez-Viejo, J. Ultrastable glasses: new perspectives for an old problem. *Nuovo Cimento* **2022**, *45* (5), 325−406.
(31) Cheng, S.; Lee, Y.; Yu, J.; Yu, L.; Ediger, M. D. Generic Behavior of Ultrastability and Anisotropic Molecular Packing in Codeposited Organic Semiconductor Glass Mixtures. *Chem. Mater.* **2024**, *36* (7), 3205−3214.
(32) Sakai, Y.; Shibata, M.; Yokoyama, D. Simple model-free estimation of orientation order parameters of vacuum-deposited and spin-coated amorphous films used in organic light-emitting diodes. *Appl. Phys. Express* **2015**, *8* (9), 096601.
(33) Bishop, C.; Bagchi, K.; Toney, M. F.; Ediger, M. D. Vapor deposition rate modifies anisotropic glassy structure of an anthracene-based organic semiconductor. *J. Chem. Phys.* **2022**, *156* (1), 014504.
(34) Vaills, Y.; Qu, T.; Micoulaut, M.; Chaimbault, F.; Boolchand, P. Direct evidence of rigidity loss and self-organization in silicate glasses. *J. Phys.: Condens. Matter* **2005**, *17* (32), 4889−4896.
(35) Lyubimov, I.; Antony, L.; Walters, D. M.; Rodney, D.; Ediger, M. D.; de Pablo, J. J. Orientational anisotropy in simulated vapor-deposited molecular glasses. *J. Chem. Phys.* **2015**, *143* (9), 094502.
(36) Jiang, J.; Walters, D. M.; Zhou, D.; Ediger, M. D. Substrate temperature controls molecular orientation in two-component vapor-deposited glasses. *Soft Matter* **2016**, *12* (13), 3265−70.
(37) Dalal, S. S.; Walters, D. M.; Lyubimov, I.; de Pablo, J. J.; Ediger, M. D. Tunable molecular orientation and elevated thermal stability of vapor-deposited organic semiconductors. *Proc. Natl. Acad. Sci. U. S. A.* **2015**, *112* (14), 4227−32.
(38) Bishop, C.; Chen, Z.; Toney, M. F.; Bock, H.; Yu, L.; Ediger, M. D. Using Deposition Rate and Substrate Temperature to Manipulate Liquid Crystal-Like Order in a Vapor-Deposited Hexagonal Columnar Glass. *J. Phys. Chem. B* **2021**, *125* (10), 2761−2770.
(39) Zhang, A.; Moore, A. R.; Zhao, H.; Govind, S.; Wolf, S. E.; Jin, Y.; Walsh, P. J.; Riggleman, R. A.; Fakhraai, Z. The role of intramolecular relaxations on the structure and stability of vapor-deposited glasses. *J. Chem. Phys.* **2022**, *156* (24), 244703.
(40) Mondal, A. Molecular library of OLED host materials—Evaluating the multiscale simulation workflow. *Chem. Phys. Rev.* **2021**, *2* (3), 031304.
(41) I. Kabir, M.; Ibarahim, Z.; Sopian, K.; Amin, N. A Review on Progress of Amorphous and Microcrystalline Silicon Thin-Film Solar Cells. *Recent Patents on Electrical Engineeringe* **2011**, *4* (1), 50−62.
(42) Lipka, T.; Moldenhauer, L.; Müller, J.; Trieu, H. K. Photonic integrated circuit components based on amorphous silicon-on-insulator technology. *Photonics Res.* **2016**, *4* (3), 126.
(43) Della Corte, F. G.; Rao, S. Use of Amorphous Silicon for Active Photonic Devices. *IEEE Trans. Electron Devices* **2013**, *60* (5), 1495−1505.
(44) Luu, V. N. Swelling of alpha-quartz induced by MeV ions irradiation: Critical dose and swelling mechanism. *J. Nucl. Mater.* **2020**, *539*, 152266.
(45) Pignatelli, I.; Kumar, A.; Field, K. G.; Wang, B.; Yu, Y.; Le Pape, Y.; Bauchy, M.; Sant, G. Direct Experimental Evidence for Differing Reactivity Alterations of Minerals following Irradiation: The Case of Calcite and Quartz. *Sci. Rep.* **2016**, *6*, 20155.
(46) Krishnan, N. M. A.; Le Pape, Y.; Sant, G.; Bauchy, M. Effect of irradiation on silicate aggregates' density and stiffness. *J. Nucl. Mater.* **2018**, *512*, 126−136.
(47) Silva, C. M.; Rosseel, T. M.; Kirkegaard, M. C. Radiation-Induced Changes in Quartz, A Mineral Analog of Nuclear Power Plant Concrete Aggregates. *Inorg. Chem.* **2018**, *57* (6), 3329−3338.
(48) Wittels, M. C. Structural behaviou of neutron irradiated quartz. *Philos. Mag.* **1957**, *2* (24), 1445−1461.
(49) Thomas, P. A.; Brodsky, M. H.; Kaplan, D.; Lepine, D. Electron spin resonance of ultrahigh vacuum evaporated amorphous silicon:In situandex situstudies. *Phys. Rev. B* **1978**, *18* (7), 3059−3073.
(50) Fredrickson, J. E.; Waddell, C. N.; Spitzer, W. G.; Hubler, G. K. Effects of thermal annealing on the refractive index of amorphous silicon produced by ion implantation. *Appl. Phys. Lett.* **1982**, *40* (2), 172−174.
(51) Sinke, W.; Warabisako, T.; Miyao, M.; Tokuyama, T.; Roorda, S.; Saris, F. W. Transient structural relaxation of amorphous silicon. *J. Non-Cryst. Solids* **1988**, *99* (2−3), 308−323.
(52) Laaziri, K.; Kycia, S.; Roorda, S.; Chicoine, M.; Robertson, J. L.; Wang, J.; Moss, S. C. High Resolution Radial Distribution Function of Pure Amorphous Silicon. *Phys. Rev. Lett.* **1999**, *82* (17), 3460−3463.
(53) Wit, L. D.; Roorda, S.; Sinke, W. C.; Saris, F. W.; Berntsen, A. J. M.; Van Der Weg, W. F. Structural Relaxation of Amorphous Silicon Induced by High Temperature Annealing. *MRS Proceedings* **1990**, *205*, 3−8.
(54) Mercure, J. F.; Karmouch, R.; Anahory, Y.; Roorda, S.; Schiettekatte, F. Dependence of the structural relaxation of

amorphous silicon on implantation temperature. *Phys. Rev. B* **2005**, *71* (13), 134205.
(55) Weeks, R. A.; Nelson, C. M. Irradiation Effects and Short-Range Order in Fused Silica and Quartz. *J. Appl. Phys.* **1960**, *31* (9), 1555−1558.
(56) Mota, F.; Caturla, M.J.; Perlado, J.M.; Ibarra, A.; León, M.; Mollá, J. Radiation Damage Modeling of Fused Silica in Fusion Systems. 2006 Conference. Accessed 2024-November-24. https://www-pub.iaea.org/MTCD/Meetings/FEC2006/it_p1-30.pdf.
(57) Douillard, L.; Duraud, J. P. Swift heavy ion amorphization of quartz — a comparative study of the particle amorphization mechanism of quartz. *Nucl. Instrum. Methods Phys. Res., Sect. B* **1996**, *107* (1−4), 212−217.
(58) Lebel, O. S.; A. Molecular Glasses: Emerging Materialsfor the Next Generation. *Adv. Mater.* **2020**, 239−258.
(59) Craig, D. The relevance of the amorphous state to pharmaceutical dosage forms: glassy drugs and freeze dried systems. *Int. J. Pharm.* **1999**, *179* (2), 179−207.
(60) Willart, J. F.; Descamps, M. Solid state amorphization of pharmaceuticals. *Mol. Pharmaceutics* **2008**, *5* (6), 905−920.
(61) Babu, N. J.; Nangia, A. Solubility Advantage of Amorphous Drugs and Pharmaceutical Cocrystals. *Cryst. Growth Des.* **2011**, *11* (7), 2662−2679.
(62) Di Martino, P.; Magnoni, F.; Vargas Peregrina, D.; Rosa Gigliobianco, M.; Censi, R.; Malaj, L. Formation, Physicochemical Characterization, and Thermodynamic Stability of the Amorphous State of Drugs and Excipients. *Curr. Pharm. Des.* **2016**, *22* (32), 4959−4974.
(63) Kissi, E. O.; Grohganz, H.; Lobmann, K.; Ruggiero, M. T.; Zeitler, J. A.; Rades, T. Glass-Transition Temperature of the beta-Relaxation as the Major Predictive Parameter for Recrystallization of Neat Amorphous Drugs. *J. Phys. Chem. B* **2018**, *122* (10), 2803−2808.
(64) Kawakami, K. Ultraslow Cooling for the Stabilization of Pharmaceutical Glasses. *J. Phys. Chem. B* **2019**, *123* (23), 4996−5003.
(65) Wang, Y.; Wang, Y.; Cheng, J.; Chen, H.; Xu, J.; Liu, Z.; Shi, Q.; Zhang, C. Recent Advances in the Application of Characterization Techniques for Studying Physical Stability of Amorphous Pharmaceutical Solids. *Crystals* **2021**, *11* (12), 1440.
(66) Zhou, X.; Blochwitz, J.; Pfeiffer, M.; Nollau, A.; Fritz, T.; Leo, K. Enhanced Hole Injection into Amorphous Hole-Transport Layers of Organic Light-Emitting Diodes Using Controlled p-Type Doping. *Adv. Funct. Mater.* **2001**, *11* (4), 310−314.
(67) Nomura, M.; Fukukawa, K.; Shibasaki, Y.; Ueda, M. New amorphous hole-transporting molecular materials: 1,1,1-Tris(4-(4-diarylaminobenzoyloxy)phenyl)ethane. *Synth. Met.* **2002**, *132* (1), 9−13.
(68) Nomura, M.; Shibasaki, Y.; Ueda, M.; Tugita, K.; Ichikawa, M.; Taniguchi, Y. New amorphous electron-transporting materials based on Tris-benzimidazoles for all wet-process OLED devices. *Synth. Met.* **2005**, *151* (3), 261−268.
(69) Moorthy, J. N.; Venkatakrishnan, P.; Natarajan, P.; Lin, Z.; Chow, T. J. Nondoped pure-blue OLEDs based on amorphous phenylenevinylene-functionalized twisted bimesitylenes. *J. Org. Chem.* **2010**, *75* (8), 2599−2609.
(70) Kim, J. Y.; Yasuda, T.; Yang, Y. S.; Adachi, C. Bifunctional star-burst amorphous molecular materials for OLEDs: achieving highly efficient solid-state luminescence and carrier transport induced by spontaneous molecular orientation. *Adv. Mater.* **2013**, *25* (19), 2666−2671.
(71) Bagchi, K.; Ediger, M. D. Controlling Structure and Properties of Vapor-Deposited Glasses of Organic Semiconductors: Recent Advances and Challenges. *J. Phys. Chem. Lett.* **2020**, *11* (17), 6935−6945.
(72) Sun, L.; Yoshida, T.; Harada, Y.; White, M.S.; Suzuri, Y. Amorphous dielectric metal-organic electron injection layer for efficient inverted organic light-emitting diodes. *Org. Electron.* **2023**, *122*, 106878.
(73) Yokoyama, D.; Qiang Wang, Z.; Pu, Y.-J.; Kobayashi, K.; Kido, J.; Hong, Z. High-efficiency simple planar heterojunction organic thin-film photovoltaics with horizontally oriented amorphous donors. *Sol. Energy Mater. Sol. Cells* **2012**, *98*, 472−475.
(74) Hedley, G. J.; Ruseckas, A.; Samuel, I. D. Light Harvesting for Organic Photovoltaics. *Chem. Rev.* **2017**, *117* (2), 796−837.
(75) Nunzi, J. M.; Lebel, O. Revisiting the Optimal Nano-Morphology: Towards Amorphous Organic Photovoltaics. *Chem. Rec.* **2019**, *19* (6), 1028−1038.
(76) Esembeson, B.; Scimeca, M. L.; Michinobu, T.; Diederich, F.; Biaggio, I. A High-Optical Quality Supramolecular Assembly for Third-Order Integrated Nonlinear Optics. *Adv. Mater.* **2008**, *20* (23), 4584−4587.
(77) Jang, S. H.; Jen, A. K. Electro-optic (E-O) molecular glasses. *Chem.—Asian J.* **2009**, *4* (1), 20−31.
(78) Traskovskis, K.; Mihailovs, I.; Tokmakovs, A.; Jurgis, A.; Kokars, V.; Rutkis, M. Triphenyl moieties as building blocks for obtaining molecular glasses with nonlinear optical activity. *J. Mater. Chem.* **2012**, *22* (22), 11268.
(79) Seniutinas, G.; Tomašiūnas, R.; Czaplicki, R.; Sahraoui, B.; Daškevičienė, M.; Getautis, V.; Balevičius, Z. Arylmethylene-1,3-indandione based molecular glasses: Third order optical non-linearity. *Dyes Pigm.* **2012**, *95* (1), 33−40.
(80) Gu, C.; Huang, Z.; Rahman, A.; Chen, X.; Zeng, Z.; Liang, Z.; Shi, L.; Liu, F.; Wang, J. Supramolecular self-assembled nonlinear optical molecular glasses with enhanced electro-optic activity and alignment stability. *Dyes Pigm.* **2022**, *202*, 110283.
(81) Biaggio, I. The Appeal of Small Molecules for Practical Nonlinear Optics. *Chemistry* **2022**, *28* (6), No. e202103168.
(82) Angell, C. A. Formation of Glasses from Liquids and Biopolymers. *Science* **1995**, *267* (5206), 1924−1935.
(83) Angell, C. A.; Ngai, K. L.; McKenna, G. B.; McMillan, P. F.; Martin, S. W. Relaxation in glassforming liquids and amorphous solids. *J. Appl. Phys.* **2000**, *88* (6), 3113−3157.
(84) Cavagna, A. Supercooled liquids for pedestrians. *Phys. Rep.* **2009**, *476* (4−6), 51−124.
(85) Lee, T. W.; Noh, T.; Shin, H. W.; Kwon, O.; Park, J. J.; Choi, B. K.; Kim, M. S.; Shin, D. W.; Kim, Y. R. Characteristics of Solution-Processed Small-Molecule Organic Films and Light-Emitting Diodes Compared with their Vacuum-Deposited Counterparts. *Adv. Funct. Mater.* **2009**, *19* (10), 1625−1630.
(86) Niu, Q.; Zhang, Q.; Xu, W.; Jiang, Y.; Xia, R.; Bradley, D. D. C.; Li, D.; Wen, X. Solution-processed anthracene-based molecular glasses as stable blue-light-emission laser gain media. *Org. Electron.* **2015**, *18*, 95−100.
(87) Gujral, A.; Yu, L.; Ediger, M. D. Anisotropic organic glasses. *Curr. Opin. Solid State Mater. Sci.* **2018**, *22* (2), 49−57.
(88) Mao, G.; Wu, Z.; He, Q.; Jiao, B.; Xu, G.; Hou, X.; Chen, Z.; Gong, Q. Considerable improvement in the stability of solution processed small molecule OLED by annealing. *Appl. Surf. Sci.* **2011**, *257* (17), 7394−7398.
(89) Feng, S.; Duan, L.; Hou, L.; Qiao, J.; Zhang, D.; Dong, G.; Wang, L.; Qiu, Y. A Comparison Study of the Organic Small Molecular Thin Films Prepared by Solution Process and Vacuum Deposition: Roughness, Hydrophilicity, Absorption, Photoluminescence, Density, Mobility, and Electroluminescence. *J. Phys. Chem. C* **2011**, *115* (29), 14278−14284.
(90) Wang, D.; Wu, Z.; Lei, X.; Zhang, W.; Jiao, B.; Wang, D.; Hou, X. Electroluminescence of solution-processed organic light-emitting diodes based on fluorescent small molecules and polymer as hole-transporting layer. *Phys. Status Solidi* **2013**, *210* (12), 2556−2560.
(91) Xing, X.; Zhong, L.; Zhang, L.; Chen, Z.; Qu, B.; Chen, E.; Xiao, L.; Gong, Q. Essential Differences of Organic Films at the Molecular Level via Vacuum Deposition and Solution Processes for Organic Light-Emitting Diodes. *J. Phys. Chem. C* **2013**, *117* (48), 25405−25408.
(92) Prakash, S.; Sims, M.; Wyrsta, I.; Parker, I. D.; Kondakov, D.; Gao, W. 49.1: Invited Paper: Solution-Processed OLEDs: Unique

Challenges and Advantages. *SID Symp. Dig. Technol. Pap.* **2013**, *44* (1), 678−681.
(93) Pfeiffer, F.; Felix, N. M.; Neuber, C.; Ober, C. K.; Schmidt, H. W. Physical Vapor Deposition of Molecular Glass Photoresists: A New Route to Chemically Amplified Patterning. *Adv. Funct. Mater.* **2007**, *17* (14), 2336−2342.
(94) Singh, S.; de Pablo, J. J. A molecular view of vapor deposited glasses. *J. Chem. Phys.* **2011**, *134* (19), 194903.
(95) Beasley, M. S.; Bishop, C.; Kasting, B. J.; Ediger, M. D. Vapor-Deposited Ethylbenzene Glasses Approach "Ideal Glass" Density. *J. Phys. Chem. Lett.* **2019**, *10* (14), 4069−4075.
(96) Jin, Y.; Zhang, A.; Wolf, S.E.; Govind, S.; Moore, A.R.; Zhernenkov, M.; Freychet, G.; Arabi Shamsabadi, A.; Fakhraai, Z. Glasses denser than the supercooled liquid. *Proc. Natl. Acad. Sci. U. S. A.* **2021**, *118* (31), e2100738118.
(97) Luo, P.; et al. High-density stable glasses formed on soft substrates. *Nat. Mater.* **2024**, *23* (5), 688−694.
(98) Kearns, K. L.; Swallen, S. F.; Ediger, M. D.; Wu, T.; Sun, Y.; Yu, L. Hiking down the energy landscape: progress toward the Kauzmann temperature via vapor deposition. *J. Phys. Chem. B* **2008**, *112* (16), 4934−4942.
(99) Ishii, K.; Yokoyama, Y.; Moriyama, R.; Nakayama, H. Liquid−Liquid Relaxation in the Supercooled Liquid State of Ethylbenzene: Thermal Studies Using a Prototype DTA Sensor for the Study of Vapor-deposited Samples. *Chem. Lett.* **2010**, *39* (9), 958−960.
(100) Kearns, K. L.; Still, T.; Fytas, G.; Ediger, M. D. High-modulus organic glasses prepared by physical vapor deposition. *Adv. Mater.* **2010**, *22* (1), 39−42.
(101) Fakhraai, Z.; Still, T.; Fytas, G.; Ediger, M. D. Structural Variations of an Organic Glassformer Vapor-Deposited onto a Temperature Gradient Stage. *J. Phys. Chem. Lett.* **2011**, *2* (5), 423−427.
(102) Wolf, S. E.; Fulco, S.; Zhang, A.; Zhao, H.; Walsh, P. J.; Turner, K. T.; Fakhraai, Z. Role of Molecular Layering in the Enhanced Mechanical Properties of Stable Glasses. *J. Phys. Chem. Lett.* **2022**, *13* (15), 3360−3368.
(103) Hellman, F. Surface-induced ordering: A model for vapor-deposition growth of amorphous materials. *Appl. Phys. Lett.* **1994**, *64* (15), 1947−1949.
(104) Yokoyama, D.; Setoguchi, Y.; Sakaguchi, A.; Suzuki, M.; Adachi, C. Orientation Control of Linear-Shaped Molecules in Vacuum-Deposited Organic Amorphous Films and Its Effect on Carrier Mobilities. *Adv. Funct. Mater.* **2010**, *20* (3), 386−391.
(105) Dawson, K. J.; Zhu, L.; Yu, L.; Ediger, M. D. Anisotropic structure and transformation kinetics of vapor-deposited indomethacin glasses. *J. Phys. Chem. B* **2011**, *115* (3), 455−463.
(106) Yokoyama, D. Molecular orientation in small-molecule organic light-emitting diodes. *J. Mater. Chem.* **2011**, *21* (48), 19187.
(107) Dawson, K.; Kopff, L. A.; Zhu, L.; McMahon, R. J.; Yu, L.; Richert, R.; Ediger, M. D. Molecular packing in highly stable glasses of vapor-deposited tris-naphthylbenzene isomers. *J. Chem. Phys.* **2012**, *136* (9), 094505.
(108) Dalal, S. S.; Ediger, M. D. Molecular Orientation in Stable Glasses of Indomethacin. *J. Phys. Chem. Lett.* **2012**, *3* (10), 1229−1233.
(109) Gujral, A.; O'Hara, K. A.; Toney, M. F.; Chabinyc, M. L.; Ediger, M. D. Structural Characterization of Vapor-Deposited Glasses of an Organic Hole Transport Material with X-ray Scattering. *Chem. Mater.* **2015**, *27* (9), 3341−3348.
(110) Gomez, J.; Jiang, J.; Gujral, A.; Huang, C.; Yu, L.; Ediger, M. D. Vapor deposition of a smectic liquid crystal: highly anisotropic, homogeneous glasses with tunable molecular orientation. *Soft. Matter.* **2016**, *12* (11), 2942−2947.
(111) Liu, T.; et al. Birefringent Stable Glass with Predominantly Isotropic Molecular Orientation. *Phys. Rev. Lett.* **2017**, *119* (9), 095502.
(112) Laventure, A.; Gujral, A.; Lebel, O.; Pellerin, C.; Ediger, M. D. Influence of Hydrogen Bonding on the Kinetic Stability of Vapor-Deposited Glasses of Triazine Derivatives. *J. Phys. Chem. B* **2017**, *121* (10), 2350−2358.
(113) Walters, D. M.; Antony, L.; de Pablo, J. J.; Ediger, M. D. Influence of Molecular Shape on the Thermal Stability and Molecular Orientation of Vapor-Deposited Organic Semiconductors. *J. Phys. Chem. Lett.* **2017**, *8* (14), 3380−3386.
(114) Sohn, S.; Park, K. H.; Kwon, S. K.; Lee, H. K.; Ahn, H.; Jung, S.; Kim, Y. H. Preferential Orientation of Tetrahedral Silicon-Based Hosts in Phosphorescent Organic Light-Emitting Diodes. *ACS Omega* **2018**, *3* (8), 9989−9996.
(115) Bagchi, K.; Jackson, N. E.; Gujral, A.; Huang, C.; Toney, M. F.; Yu, L.; de Pablo, J. J.; Ediger, M. D. Origin of Anisotropic Molecular Packing in Vapor-Deposited Alq3 Glasses. *J. Phys. Chem. Lett.* **2019**, *10* (2), 164−170.
(116) Ediger, M. D.; de Pablo, J.; Yu, L. Anisotropic Vapor-Deposited Glasses: Hybrid Organic Solids. *Acc. Chem. Res.* **2019**, *52* (2), 407−414.
(117) Oh-e, M.; Ogata, H.; Araoka, F. Randomization and Constraint of Molecular Alignment and Orientation: Temperature-Dependent Anisotropy and Phase Transition in Vapor-Deposited Thin Films of an Organic Cross-Shaped Molecule. *ACS Omega* **2019**, *4* (1), 39−47.
(118) Mikaeili, A.; Matsushima, T.; Esaki, Y.; Yazdani, S. A.; Adachi, C.; Mohajerani, E. The origin of changes in electrical properties of organic films fabricated at various vacuum-deposition rates. *Opt. Mater.* **2019**, *91*, 93−100.
(119) Cang, Y.; Wang, Z.; Bishop, C.; Yu, L.; Ediger, M.D.; Fytas, G. Extreme Elasticity Anisotropy in Molecular Glasses. *Adv. Funct. Mater.* **2020**, *30* (23), 2001481.
(120) Thelen, J. L.; et al. Molecular Orientation Depth Profiles in Organic Glasses Using Polarized Resonant Soft X-ray Reflectivity. *Chem. Mater.* **2020**, *32* (15), 6295−6309.
(121) Tanaka, M.; Noda, H.; Nakanotani, H.; Adachi, C. Molecular orientation of disk-shaped small molecules exhibiting thermally activated delayed fluorescence in host−guest films. *Appl. Phys. Lett.* **2020**, *116* (2), 023302.
(122) Bishop, C.; Li, Y.; Toney, M. F.; Yu, L.; Ediger, M. D. Molecular Orientation for Vapor-Deposited Organic Glasses Follows Rate-Temperature Superposition: The Case of Posaconazole. *J. Phys. Chem. B* **2020**, *124* (12), 2505−2513.
(123) Ferron, T. J.; Thelen, J. L.; Bagchi, K.; Deng, C.; Gann, E.; de Pablo, J. J.; Ediger, M. D.; Sunday, D. F.; DeLongchamp, D. M. Characterization of the Interfacial Orientation and Molecular Conformation in a Glass-Forming Organic Semiconductor. *ACS Appl. Mater. Interfaces* **2022**, *14* (2), 3455−3466.
(124) Ferron, T. J.; Fiori, M. E.; Ediger, M. D.; DeLongchamp, D. M.; Sunday, D. F. Composition Dictates Molecular Orientation at the Heterointerfaces of Vapor-Deposited Glasses. *JACS Au* **2023**, *3* (7), 1931−1938.
(125) Bishop, C.; Thelen, J. L.; Gann, E.; Toney, M. F.; Yu, L.; DeLongchamp, D. M.; Ediger, M. D. Vapor deposition of a nonmesogen prepares highly structured organic glasses. *Proc. Natl. Acad. Sci. U. S. A.* **2019**, *116* (43), 21421−21426.
(126) Stevenson, J. D.; Wolynes, P. G. On the surface of glasses. *J. Chem. Phys.* **2008**, *129* (23), 234514.
(127) Yu, L. Surface mobility of molecular glasses and its importance in physical stability. *Adv. Drug. Delivery Rev.* **2016**, *100*, 3−9.
(128) Samanta, S.; et al. Exploring the Importance of Surface Diffusion in Stability of Vapor-Deposited Organic Glasses. *J. Phys. Chem. B* **2019**, *123* (18), 4108−4117.
(129) Chen, Y.; Chen, Z.; Tylinski, M.; Ediger, M. D.; Yu, L. Effect of molecular size and hydrogen bonding on three surface-facilitated processes in molecular glasses: Surface diffusion, surface crystal growth, and formation of stable glasses by vapor deposition. *J. Chem. Phys.* **2019**, *150* (2), 024502.
(130) Fiori, M. E.; Bagchi, K.; Toney, M.F.; Ediger, M.D. Surface equilibration mechanism controls the molecular packing of glassy molecular semiconductors at organic interfaces. *Proc. Natl. Acad. Sci. U. S. A.* **2021**, *118* (42), e2111988118.

(131) Luo, P.; Fakhraai, Z. Surface-Mediated Formation of Stable Glasses. *Annu. Rev. Phys. Chem.* **2023**, *74*, 361−389.
(132) Mayr, C.; Brütting, W. Control of Molecular Dye Orientation in Organic Luminescent Films by the Glass Transition Temperature of the Host Material. *Chem. Mater.* **2015**, *27* (8), 2759−2762.
(133) Liu, H.; Zhao, Z.; Zhou, Q.; Chen, R.; Yang, K.; Wang, Z.; Tang, L.; Bauchy, M. Challenges and opportunities in atomistic simulations of glasses: a review. *C.R. GEOSCI.* **2022**, *354* (S1), 35−77.
(134) Du, J., Challenges in Molecular Dynamics Simulations of Multicomponent Oxide Glasses In *Molecular Dynamics Simulations of Disordered Materials: From Network Glasses to Phase-Change Memory Alloys*; Massobrio, C. et al, Eds.; 2015, Springer International Publishing: Cham. p 157−180.
(135) Horbach, J.; Kob, W.; Binder, K.; Angell, C. A. Finite size effects in simulations of glass dynamics. *Phys. Rev. E Stat. Phys. Plasmas Fluids Relat. Interdiscip. Topics* **1996**, *54* (6), R5897−R5900.
(136) Berthier, L.; Biroli, G.; Coslovich, D.; Kob, W.; Toninelli, C. Finite-size effects in the dynamics of glass-forming liquids. *Phys. Rev. E. Stat. Nonlin. Soft Matter. Phys.* **2012**, *86* (3 Pt 1), 031502.
(137) Du, J. Molecular dynamics simulations of oxide glasses. In *Springer Handbook of Glass*; Musgraves, J. D., Hu, J.; Calvez, L., Eds.; Springer International Publishing, Cham, 2019; pp 1131−1155.
(138) Leach, A. R. *Molecular Modelling: Principles and Applications*; Prentice Hall, New York. 2001.
(139) Ganster, P.; Benoit, M.; Kob, W.; Delaye, J. M. Structural properties of a calcium aluminosilicate glass from molecular-dynamics simulations: a finite size effects study. *J. Chem. Phys.* **2004**, *120* (21), 10172−10181.
(140) Nakano, A.; Kalia, R. K.; Vashishta, P. First sharp diffraction peak and intermediate-range order in amorphous silica: finite-size effects in molecular dynamics simulations. *J. Non-Cryst. Solids* **1994**, *171* (2), 157−163.
(141) van Duin, A. C. T.; Strachan, A.; Stewman, S.; Zhang, Q.; Xu, X.; Goddard, W. A. ReaxFFSiO Reactive Force Field for Silicon and Silicon Oxide Systems. *J. Phys. Chem. A* **2003**, *107* (19), 3803−3811.
(142) Liu, H.; Fu, Z.; Li, Y.; Sabri, N. F. A.; Bauchy, M. Balance between accuracy and simplicity in empirical forcefields for glass modeling: Insights from machine learning. *J. Non-Cryst. Solids* **2019**, *515*, 133−142.
(143) Massobrio, C., Du, J.; Bernasconi, M.; Salmon, P.S. *Molecular Dynamics Simulations of Disordered Materials: From Network Glasses to Phase-Change Memory Alloys*; Springer International Publishing, 2015.
(144) Shewchuk, J. R. An Introduction to the Conjugate Gradient Method Without the Agonizing Pain, 1994. Carnegie Mellon University, United States. https://www.cs.cmu.edu/%7Equake-papers/painless-conjugate-gradient.pdf.
(145) Liu, H.; Fu, Z.; Li, Y.; Sabri, N. F. A.; Bauchy, M. Parameterization of empirical forcefields for glassy silica using machine learning. *MRS Commun.* **2019**, *9* (2), 593−599.
(146) Thorpe, M. F. Continuous deformations in random networks. *J. Non Cryst. Solids* **1983**, *57* (3), 355−370.
(147) Horbach, J.; Kob, W. Static and dynamic properties of a viscous silica melt. *Phys. Rev. B* **1999**, *60* (5), 3169−3181.
(148) Zaccone, A. *Theory of Disordered Solids*; Lecture Notes in Physics; Springer: Cham, 2023.
(149) Lewis, L. J. Fifty years of amorphous silicon models: the end of the story? *J. Non Cryst. Solids* **2022**, *580*, 121383.
(150) Micoulaut, M.; Bauchy, M. Topology and Rigidity of Silicate Melts and Glasses. *Rev. Mineral. Geochem.* **2022**, *87* (1), 163−191.
(151) Polk, D. E. Structural model for amorphous silicon and germanium. *J. Non Cryst. Solids* **1971**, *5* (5), 365−376.
(152) Wooten, F.; Winer, K.; Weaire, D. Computer generation of structural models of amorphous Si and Ge. *Phys. Rev. Lett.* **1985**, *54* (13), 1392−1395.
(153) Keating, P. N. Effect of Invariance Requirements on the Elastic Strain Energy of Crystals with Application to the Diamond Structure. *Phys. Rev.* **1966**, *145* (2), 637−645.
(154) Djordjevic, B. R.; Thorpe, M. F.; Wooten, F. Computer model of tetrahedral amorphous diamond. *Phys. Rev. B Condens. Matter.* **1995**, *52* (8), 5685−5689.
(155) Barkema, G. T.; Mousseau, N. High-quality continuous random networks. *Phys. Rev. B* **2000**, *62* (8), 4985−4990.
(156) Vink, R. L. C.; Barkema, G. T.; Stijnman, M. A.; Bisseling, R. H. Device-size atomistic models of amorphous silicon. *Phys. Rev. B* **2001**, *64* (24), 245214.
(157) Stillinger, F. H.; Weber, T. A. Computer simulation of local order in condensed phases of silicon. *Phys. Rev. B Condens. Matter.* **1985**, *31* (8), 5262−5271.
(158) Vink, R. L. C.; Barkema, G. T.; van der Weg, W. F.; Mousseau, N. Fitting the Stillinger−Weber potential to amorphous silicon. *J. Non Cryst. Solids* **2001**, *282* (2−3), 248−255.
(159) Hejna, M.; Steinhardt, P. J.; Torquato, S. Nearly hyperuniform network models of amorphous silicon. *Phys. Rev. B* **2013**, *87* (24), 245204.
(160) Mousseau, N.; Barkema, G. T. Binary continuous random networks. *J. Phys.: Condens. Matter* **2004**, *16* (44), S5183−S5190.
(161) Laaziri, K.; Kycia, S.; Roorda, S.; Chicoine, M.; Robertson, J. L.; Wang, J.; Moss, S. C. High-energy x-ray diffraction study of pure amorphous silicon. *Phys. Rev. B* **1999**, *60* (19), 13520−13533.
(162) Ovshinsky, S. R. Localized States in the Gap of Amorphous Semiconductors. *Phys. Rev. Lett.* **1976**, *36* (24), 1469−1472.
(163) Pandey, K. C. Newπ-Bonded Chain Model for Si(111)-(2 × 1) Surface. *Phys. Rev. Lett.* **1981**, *47* (26), 1913−1917.
(164) Srolovitz, D.; Maeda, K.; Vitek, V.; Egami, T. Structural defects in amorphous solids Statistical analysis of a computer model. *Philos. Mag. A* **1981**, *44* (4), 847−866.
(165) Adler, D. Normal structural bonding and defects in covalent amorphous solids. *J. Solid State Chem.* **1982**, *45* (1), 40−50.
(166) Rucavado, E.; et al. Enhancing the optoelectronic properties of amorphous zinc tin oxide by subgap defect passivation: A theoretical and experimental demonstration. *Phys. Rev. B* **2017**, *95* (24), 245204.
(167) Newnham, R. E.; Sundar, V.; Yimnirun, R.; Su, J.; Zhang, Q. M. Electrostriction: Nonlinear Electromechanical Coupling in Solid Dielectrics. *J. Phys. Chem. B* **1997**, *101* (48), 10141−10150.
(168) Egami, T.; Maeda, K.; Vitek, V. Structural defects in amorphous solids A computer simulation study. *Philos. Mag. A* **1980**, *41* (6), 883−901.
(169) Paret, J.; Jack, R. L.; Coslovich, D. Assessing the structural heterogeneity of supercooled liquids through community inference. *J. Chem. Phys.* **2020**, *152* (14), 144502.
(170) Tanguy, A.; Mantisi, B.; Tsamados, M. Vibrational modes as a predictor for plasticity in a model glass. *EPL (Europhysics Letters)* **2010**, *90* (1), 16004.
(171) Manning, M. L.; Liu, A. J. Vibrational modes identify soft spots in a sheared disordered packing. *Phys. Rev. Lett.* **2011**, *107* (10), 108302.
(172) Pusztai, L.; Kugler, S. Reverse Monte Carlo simulation: the structure of amorphous silicon. *J. Non-Cryst. Solids* **1993**, *164−166*, 147−150.
(173) McGreevy, R. L.; Pusztai, L. Reverse Monte Carlo Simulation: A New Technique for the Determination of Disordered Structures. *Mol. Simul.* **1988**, *1* (6), 359−367.
(174) McGreevy, R. L.; Howe, M. A. RMC: Modeling Disordered Structures. *Annu. Rev. Mater. Sci.* **1992**, *22* (1), 217−242.
(175) Biswas, P.; Atta-Fynn, R.; Drabold, D. A. Reverse Monte Carlo modeling of amorphous silicon. *Phys. Rev. B* **2004**, *69* (19), 195207.
(176) Pandey, A.; Biswas, P.; Drabold, D.A. Force-enhanced atomic refinement: Structural modeling with interatomic forces in a reverse Monte Carlo approach applied to amorphous Si and SiO2. *Phys. Rev. B* **2015**, *92* (15), 155205.
(177) Pandey, A.; Biswas, P.; Drabold, D. A. Inversion of diffraction data for amorphous materials. *Sci. Rep.* **2016**, *6* (1), 33731.
(178) Pandey, A.; Biswas, P.; Bhattarai, B.; Drabold, D. A. Realistic inversion of diffraction data for an amorphous solid: The case of amorphous silicon. *Phys. Rev. B* **2016**, *94* (23), 235208.

(179) Igram, D.; Bhattarai, B.; Biswas, P.; Drabold, D. A. Large and realistic models of amorphous silicon. *J. Non Cryst. Solids* **2018**, *492*, 27−32.
(180) Barkema, G. T.; Mousseau, N. Event-Based Relaxation of Continuous Disordered Systems. *Phys. Rev. Lett.* **1996**, *77* (21), 4358−4361.
(181) Malek, R.; Mousseau, N. Dynamics of lennard-jones clusters: A characterization of the activation-relaxation technique. *Phys. Rev. E Stat. Phys. Plasmas Fluids Relat. Interdiscip. Topics* **2000**, *62* (6 Pt A), 7723−7728.
(182) Mousseau, N.; Barkema, G. T. Traveling through potential energy landscapes of disordered materials: The activation-relaxation technique. *Phys. Rev. E* **1998**, *57* (2), 2419−2424.
(183) Kallel, H.; Mousseau, N.; Schiettekatte, F. Evolution of the potential-energy surface of amorphous silicon. *Phys. Rev. Lett.* **2010**, *105* (4), 045503.
(184) Mousseau, N.; Lewis, L. J. Topology of Amorphous Tetrahedral Semiconductors on Intermediate Length Scales. *Phys. Rev. Lett.* **1997**, *78* (8), 1484−1487.
(185) Mousseau, N.; Barkema, G. T.; de Leeuw, S. W. Elementary mechanisms governing the dynamics of silica. *J. Chem. Phys.* **2000**, *112* (2), 960−964.
(186) Mousseau, N.; Barkema, G. T. Activated mechanisms in amorphous silicon: An activation-relaxation-technique study. *Phys. Rev. B* **2000**, *61* (3), 1898−1906.
(187) Grigera, T. S.; Parisi, G. Fast Monte Carlo algorithm for supercooled soft spheres. *Phys. Rev. E Stat. Nonlin. Soft. Matter. Phys.* **2001**, *63* (4Pt 2), 045102.
(188) Berthier, L.; Biroli, G.; Bouchaud, J.-P.; Tarjus, G. Can the glass transition be explained without a growing static length scale? *J. Chem. Phys.* **2019**, *150* (9), 094501.
(189) Brumer, Y.; Reichman, D. R. Numerical Investigation of the Entropy Crisis in Model Glass Formers. *J. Phys. Chem. B* **2004**, *108* (21), 6832−6837.
(190) Fernández, L. A.; Martín-Mayor, V.; Verrocchio, P. Optimized Monte Carlo method for glasses. *Philos. Mag.* **2007**, *87* (3−5), 581−586.
(191) Ninarello, A.; Berthier, L.; Coslovich, D. Models and Algorithms for the Next Generation of Glass Transition Studies. *Phys. Rev. X* **2017**, *7* (2), 021039.
(192) Scalliet, C.; Guiselin, B.; Berthier, L. Thirty Milliseconds in the Life of a Supercooled Liquid. *Phys. Rev. X* **2022**, *12* (4), 041028.
(193) Gutiérrez, R.; Karmakar, S.; Pollack, Y. G.; Procaccia, I. The static lengthscale characterizing the glass transition at lower temperatures. *EPL* **2015**, *111* (5), 56009.
(194) Parmar, A. D. S.; Ozawa, M.; Berthier, L. Ultrastable Metallic Glasses In Silico. *Phys. Rev. Lett.* **2020**, *125* (8), 085505.
(195) Fullerton, C. J.; Berthier, L. Density controls the kinetic stability of ultrastable glasses. *EPL* **2017**, *119* (3), 36003.
(196) Bojesen, T. A. Policy-guided Monte Carlo: Reinforcement-learning Markov chain dynamics. *Phys. Rev. E* **2018**, *98* (6), 063303.
(197) Gabrie, M.; Rotskoff, G. M.; Vanden-Eijnden, E. Adaptive Monte Carlo augmented with normalizing flows. *Proc. Natl. Acad. Sci. U. S. A.* **2022**, *119* (10), No. e2109420119.
(198) Galliano, L.; Rende, R.; Coslovich, D. Policy-guided Monte Carlo on general state spaces: Application to glass-forming mixtures. *J. Chem. Phys.* **2024**, *161* (6), 064503.
(199) Deringer, V. L.; Caro, M. A.; Csanyi, G. Machine Learning Interatomic Potentials as Emerging Tools for Materials Science. *Adv. Mater.* **2019**, *31* (46), No. e1902765.
(200) Caro, M. A. Machine learning based modeling of disordered elemental semiconductors: understanding the atomic structure of a-Si and a-C. *Semicond. Sci. Technol.* **2023**, *38* (4), 043001.
(201) Behler, J.; Parrinello, M. Generalized neural-network representation of high-dimensional potential-energy surfaces. *Phys. Rev. Lett.* **2007**, *98* (14), 146401.
(202) Zuo, Y.; et al. Performance and Cost Assessment of Machine Learning Interatomic Potentials. *J. Phys. Chem. A* **2020**, *124* (4), 731−745.
(203) Mishin, Y. Machine-learning interatomic potentials for materials science. *Acta Mater.* **2021**, *214*, 116980.
(204) Wang, G.; Wang, C.; Zhang, X.; Li, Z.; Zhou, J.; Sun, Z. Machine learning interatomic potential: Bridge the gap between small-scale models and realistic device-scale simulations. *iScience* **2024**, *27* (5), 109673.
(205) Khorshidi, A.; Peterson, A. A. Amp: A modular approach to machine learning in atomistic simulations. *Comput. Phys. Commun.* **2016**, *207*, 310−324.
(206) Bartók, A. P.; Kermode, J.; Bernstein, N.; Csányi, G. Machine Learning a General-Purpose Interatomic Potential for Silicon. *Phys. Rev. X* **2018**, *8* (4), 195207.
(207) Thompson, A. P.; Swiler, L. P.; Trott, C. R.; Foiles, S. M.; Tucker, G. J. Spectral neighbor analysis method for automated generation of quantum-accurate interatomic potentials. *J. Comput. Phys.* **2015**, *285*, 316−330.
(208) Shapeev, A. V. Moment Tensor Potentials: A Class of Systematically Improvable Interatomic Potentials. *Multiscale Model. Sim.* **2016**, *14* (3), 1153−1173.
(209) Deringer, V. L.; Bernstein, N.; Bartok, A. P.; Cliffe, M. J.; Kerber, R. N.; Marbella, L. E.; Grey, C. P.; Elliott, S. R.; Csanyi, G. Realistic Atomistic Structure of Amorphous Silicon from Machine-Learning-Driven Molecular Dynamics. *J. Phys. Chem. Lett.* **2018**, *9* (11), 2879−2885.
(210) Bartók, A. P.; Kermode, J.; Bernstein, N.; Csányi, G. Machine Learning a General-Purpose Interatomic Potential for Silicon. *Phys. Rev. X* **2018**, *8* (4), 041048.
(211) Bernstein, N.; Bhattarai, B.; Csanyi, G.; Drabold, D. A.; Elliott, S. R.; Deringer, V. L. Quantifying Chemical Structure and Machine-Learned Atomic Energies in Amorphous and Liquid Silicon. *Angew. Chem., Int. Ed. Engl.* **2019**, *58* (21), 7057−7061.
(212) Erhard, L. C.; Rohrer, J.; Albe, K.; Deringer, V. L. A machine-learned interatomic potential for silica and its relation to empirical models. *npj Comput. Mater.* **2022**, *8* (1), 90.
(213) Erhard, L. C.; Rohrer, J.; Albe, K.; Deringer, V. L. Modelling atomic and nanoscale structure in the silicon−oxygen system through active machine learning. *Nat. Commun.* **2024**, *15* (1), 1927.
(214) Drautz, R. Atomic cluster expansion for accurate and transferable interatomic potentials. *Phys. Rev. B* **2019**, *99* (1), 249901.
(215) Zongo, K.; Sun, H.; Ouellet-Plamondon, C.; Béland, L. K. A unified moment tensor potential for silicon, oxygen, and silica. *npj Comput. Mater.* **2024**, *10* (1), 218.
(216) Zongo, K.; Béland, L. K.; Ouellet-Plamondon, C. First-principles database for fitting a machine-learning silicon interatomic force field. *MRS Adv.* **2022**, *7* (2−3), 39−47.
(217) Morrow, J. D.; Ugwumadu, C.; Drabold, D. A.; Elliott, S. R.; Goodwin, A. L.; Deringer, V. L. Understanding Defects in Amorphous Silicon with Million-Atom Simulations and Machine Learning. *Angew. Chem., Int. Ed. Engl.* **2024**, *63* (22), No. e202403842.
(218) Atta-Fynn, R.; Biswas, P. Nearly defect-free dynamical models of disordered solids: The case of amorphous silicon. *J. Chem. Phys.* **2018**, *148* (20), 204503.
(219) Comin, M.; Lewis, L. J. Deep-learning approach to the structure of amorphous silicon. *Phys. Rev. B* **2019**, *100* (9), 094107.
(220) Mills, K.; Casert, C.; Tamblyn, I. Adversarial Generation of Mesoscale Surfaces from Small-Scale Chemical Motifs. *J. Phys. Chem. C* **2020**, *124* (42), 23158−23163.
(221) Zhou, Z.; Shang, Y.; Liu, X.; Yang, Y. A generative deep learning framework for inverse design of compositionally complex bulk metallic glasses. *npj Comput. Mater.* **2023**, *9* (1), 15.
(222) Invernizzi, M.; Kramer, A.; Clementi, C.; Noe, F. Skipping the Replica Exchange Ladder with Normalizing Flows. *J. Phys. Chem. Lett.* **2022**, *13* (50), 11643−11649.
(223) Kilgour, M.; Gastellu, N.; Hui, D. Y. T.; Bengio, Y.; Simine, L. Generating Multiscale Amorphous Molecular Structures Using Deep Learning: A Study in 2D. *J. Phys. Chem. Lett.* **2020**, *11* (20), 8532−8537.
(224) Madanchi, A.; Kilgour, M.; Zysk, F.; Kühne, T. D.; Simine, L. Simulations of Disordered Matter in 3D with the Morphological

Autoregressive Protocol (MAP) and Convolutional Neural Networks. *J. Chem. Phys.* **2024**, 024101.
(225) Wang, H., Jiang, Z.; Yi, L.; Mo, K.; Su, H.; Guibas, L. Rethinking Sampling in 3D Point Cloud Generative Adversarial Networks. *arXiv*, 12 Jun 2020. DOI: 10.48550/arXiv.2006.07029 (accessed 2024-November-24).
(226) Charles, R. Q., Su, H., Kaichun, M., Guibas, L. J.. PointNet: Deep Learning on Point Sets for 3D Classification and Segmentation. In *IEEE Conference on Computer Vision and Pattern Recognition (CVPR)*. 2017 Conference. DOI: 10.1109/CVPR.2017.16.
(227) Zhou, Q.; Du, T.; Guo, L.; Smedskjaer, M.M.; Bauchy, M. New insights into the structure of sodium silicate glasses by force-enhanced atomic refinement. *J. Non-Cryst. Solids* **2020**, *536*, 120006.
(228) Santos, I.; Aboy, M.; Marqués, L. A.; López, P.; Pelaz, L. Generation of amorphous Si structurally compatible with experimental samples through the quenching process: A systematic molecular dynamics simulation study. *J. Non-Cryst. Solids* **2019**, *503*−*504*, 20−27.
(229) Cooper, N. C.; Goringe, C. M.; McKenzie, D. R. Density functional theory modelling of amorphous silicon. *Comput. Mater. Sci.* **2000**, *17* (1), 1−6.
(230) Marques, L. A.; Pelaz, L.; Santos, I.; Bail6n, L.; Barbolla, J.. Study of the amorphous phase of silicon using molecular dynamics simulation techniques. In *Conference on Electron Devices*. 2005 Conference. DOI: 10.1109/SCED.2005.1504416.
(231) Sundararaman, S.; Huang, L.; Ispas, S.; Kob, W. New optimization scheme to obtain interaction potentials for oxide glasses. *J. Chem. Phys.* **2018**, *148* (19), 194504.
(232) Giacovazzo, C. *Fundamentals of crystallography*; Oxford university press, 2002; Vol. *7*.
(233) Pecharsky, V. K.; Zavalij, P. Y. *Fundamentals of Powder Diffraction and Structural Characterization of Materials*; Springer: New York, 2009.
(234) Zhang, N.; Yokota, H.; Glazer, A. M.; Thomas, P. A. Neutron powder diffraction refinement of PbZr(1 - x)Ti(x)O3. *Acta. Crystallogr. B* **2011**, *67* (Pt 5), 386−398.
(235) Kisi, E. H.; Howard, C.J. *Applications of Neutron Powder Diffraction*; Oxford University Press, 2008.
(236) Li, W.; Ando, Y. Comparison of different machine learning models for the prediction of forces in copper and silicon dioxide. *Phys. Chem. Chem. Phys.* **2018**, *20* (47), 30006−30020.
(237) Balyakin, I. A.; Rempel, S. V.; Ryltsev, R. E.; Rempel, A. A. Deep machine learning interatomic potential for liquid silica. *Phys. Rev. E* **2020**, *102* (5−1), 052125.
(238) Gereben, O.; Pusztai, L. Structure of amorphous semiconductors: Reverse Monte Carlo studies on a-C, a-Si, and a-Ge. *Phys. Rev. B. Condens. Matter.* **1994**, *50* (19), 14136−14143.
(239) Biswas, P.; Tafen, D. N.; Atta-Fynn, R.; Drabold, D. The inclusion of experimental information in first principles modelling of materials. *J. Phys.: Condens. Matter* **2004**, *16* (44), S5173−S5182.
(240) Opletal, G.; Petersen, T. C.; O'Malley, B.; Snook, I. K.; McCulloch, D. G.; Yarovsky, I. HRMC: Hybrid Reverse Monte Carlo method with silicon and carbon potentials. *Comput. Phys. Commun.* **2008**, *178* (10), 777−787.
(241) Opletal, G.; Petersen, T. C.; McCulloch, D. G.; Snook, I. K.; Yarovsky, I. The structure of disordered carbon solids studied using a hybrid reverse Monte Carlo algorithm. *J. Phys.: Condens. Matter* **2005**, *17* (17), 2605−2616.
(242) Singh, R.; ZetterstrÖM, P. E. R.; Mohan, I.; Ahluwalia, P. K. Structural Properties of Amorphous Silicon Models Generated with Reverse Monte-Carlo Method. *International Journal of Modern Physics B* **2006**, *20* (07), 779−790.
(243) Tucker, M. G.; Keen, D. A.; Dove, M. T.; Trachenko, K. Refinement of the Si−O−Si bond angle distribution in vitreous silica. *J. Phys.: Condens. Matter* **2005**, *17* (5), S67−S75.
(244) Biswas, P.; Tafen, D. N.; Drabold, D. A. Experimentally constrained molecular relaxation: The case of glassyGeSe2. *Phys. Rev. B* **2005**, *71* (5), 054204.
(245) Treacy, M. M.; Borisenko, K. B. The local structure of amorphous silicon. *Science* **2012**, *335* (6071), 950−953.